CHEMIJA
2025. Vol. 36. No. 2. P. 45–57

ISSN 0235-7216 eISSN 2424-4538
DOI: https://doi.org/10.6001/chemija.2025.36.2.1

# Structural analysis of 1-chlorosilacyclopentane by means of vibrational spectroscopy

**J. Mačytė**[1],

**J. Lach**[1],

**R. Platakytė**[1],

**J. Čeponkus**[1],

**V. Aleksa**[1],

**M. Ali**[3],

**V. Šablinskas**[1*],

**P. Rodziewicz**[2],

**G. A. Guirgis**[3*]

[1] *Institute of Chemical Physics,*
*Faculty of Physics,*
*Vilnius University,*
*3 Saulėtekio Avenue,*
*10257 Vilnius, Lithuania*

[2] *Institute of Chemistry,*
*Jan Kochanowski University,*
*15 G Swietokrzyska Street,*
*25-406 Kielce, Poland*

[3] *Department of Chemistry*
*and Biochemistry,*
*College of Charleston,*
*Charleston, SC 29424, USA*

The structure of the newly synthesised compound, 1-chlorosilacyclopentane (1-ClSiCP), was investigated using vibrational spectroscopy and theoretical calculations. ATR FT-IR and Raman spectroscopy were used to analyse the liquid sample. Matrix isolation FT-IR spectroscopy was used for the analysis of closely located infrared spectral bands of 1-ClSiCP. Spectroscopic data analysis was performed using theoretical methods such as density functional theory (DTF) and *ab initio* calculations. FT-IR spectra of 1-ClSiCP isolated in Ne and $N_2$ matrices were collected before and after annealing. During the theoretical structural analysis, the envelope ($^1E$) and twisted ($^2T_3$) ring shapes, with the chlorine atom in axial and equatorial positions, were investigated utilising the aug-cc-pVTZ basis set included in the MP2 and DFT calculations. Potential energy surface scans were performed to trace the energy changes and the structure of transition states during the ring conversion. Depending on the method applied, the theoretical results indicate the presence of different conformers, including twisted and envelope ring shapes. The experimental results confirm the existence of only one conformer in the twisted ring configuration. Good agreement between the experimental matrix isolation spectra and in the anharmonic approximation calculated IR absorption spectrum of the $^2T_3$ conformer is observed. The difference between the calculated and experimental frequencies of the normal modes does not exceed 2%.

**Keywords:** 1-chlorosilacyclopentane, matrix isolation, infrared spectroscopy, Raman spectroscopy, conformational analysis, MP2, DFT

## INTRODUCTION

Organosilicon cyclic compounds, due to their good surface adhesion properties, have a potential use as a glass surface coating [1]. The introduction of a silicon atom to the ring enhances adhesion by covalent bonding with glass. The substitution of the ring hydrogen atoms with radicals (e.g. halogen atoms, methyl groups, etc.) improves the hydrophobic properties of the compounds [2, 3]. Such an effect depends on the ring size, the type of substituents, and the conformational diversity of the molecule. Additionally, five-membered heterocycles are essential structural components in various antibacterial drugs; the physicochemical properties of a five-membered heterocycle can play a crucial role in determining the biological activity of an antibacterial drug. These properties can affect

---

[*] Corresponding author. Email: valdas.sablinskas@ff.vu.lt

the drug's activity spectrum, potency, and pharmacokinetic and toxicological properties [4]. That is why structural and spectroscopic analysis plays a crucial role in the understanding of the chemistry of heterocyclic organic molecules [5]. The dynamics and pathways of conformational rearrangements have a strong influence on molecular properties, such as chemical [6] or biological [7] activity. Moreover, it is very important that substitution, even with small radicals, can be essential for the aforementioned properties [8, 9]. A detailed literature review on heterocyclic five-member ring molecules was published in our previous work on 1-chloromethyl-1-fluorosilacyclopentane, as well as a pseudo rotation phenomenon description [10]. It is well known that cyclopentane, under experimental conditions, is most abundant in the transition state structure between twisted and envelope conformers, which is the proof of the fast conformer interchange called pseudo rotation [11, 12]. Monosubstituted silacyclopentanes with halogen atoms (Br, F) such as 1-bromosilacyclopentane and 1-fluorosilacyclopentane have only one twisted conformer [13–17], with a preferable pseudo-axial position. In substituted silacyclopentanes, alkyl groups prefer the pseudo-equatorial conformation [18]. Silacyclopentanes with two substituents have one stable ring conformation, namely twisted [19], while the envelope structure is a transition state corresponding to the saddle point of the potential energy surface.

1-chlorosilacyclopentane was synthesised recently for the first time at the College of Charleston, USA. This molecular compound might be potentially used for the fabrication of novel hydrophobic coatings. Therefore, in this work, we investigated the geometric structure and conformational properties of this compound using vibrational spectroscopy and density functional theory (DFT) and MP2 calculations. Similarly to our previous experimental and computational studies on substituted silacyclomolecules [10, 20–22], the aim of this study was the assignment of experimental vibrational spectral bands and the elucidation of structural parameters.

Generally, five-membered saturated cyclic organic molecules exist in the envelope ($C_s$) or twisted ($C_2$) conformations. The introduction of a heteroatom into the ring, along with radicals attached to the heteroatom, according to the theory, produces many possible canonical ring conformations, whose stability can differ significantly [9].

## EXPERIMENTAL

The aim of our study is to analyse 1-chlorosilacyclopentane (1-ClSiCP) using theoretical calculations and experimental vibrational spectroscopy. All calculations were performed with the ORCA 4.1.1 software package [23]. The total energies and anharmonic vibrational frequencies for 1-ClSiCP conformers were calculated. During the structural calculations, density functional theory (DFT) with the B3LYP [24] hybrid functional and Dunning's augmented double and triple zeta correlation-consistent basis set were used [25]. The molecular structure was optimised at every step during the potential energy scan. The anharmonic vibrational analysis was performed utilising B3LYP/aug-cc-pVTZ and MP2/aug-cc-pVTZ methods implemented in the GAUSSIAN program package [26]. Due to the fact that calculations of the interconversion barriers between the conformers take much computing time, they were performed using only the B3LYP/aug-cc-pVTZ method. In our current study, we describe the energetic properties of isolated molecules, therefore, we calculated the relative energies of the staggered structures, considering that the relative energy of the most stable conformer corresponds to the global minimum of potential energy surface equal to 0 kJ/mol. The two lowest-energy local minima were reoptimised using the MP2/aug-cc-pVTZ method to validate the results obtained from the DFT based calculations. For the theoretically calculated structures, the vibrational frequency analysis was performed. The Vibrational Mode Automatic Relevance Determination (VMARD) method was used to describe computationally predicted normal vibrational modes for the spectra obtained with the B3LYP/aug-cc-pVTZ method. The Automatic Relevance Determination (ARD) method for Bayesian Ridge Regression was used since it provides a good prediction of the most prominent internal coordinates [27].

Infrared absorption spectra of the title compound in the liquid phase were obtained using the attenuated total reflection (ATR) method. The spectrometer employed during those experiments was the Bruker Alpha with a single reflection ATR diamond accessory, a globar source and a DTGS detector. The spectra were recorded at 4 $cm^{-1}$ resolution.

The sample was highly volatile, and just 16 scans were averaged during the measurement. Raman spectra of the compound were recorded using a FT-Raman spectrometer, MultiRAM from Bruker (Bruker Optik GmbH, Ettlingen, Germany). The measurements were performed using a Nd:YAG (1064 nm) laser as an excitation source and a liquid nitrogen cooled germanium diode as a detector. The laser power was set to 1000 mW. Spectra were recorded with 4 $cm^{-1}$ resolution and 200 scans were averaged.

Matrix isolated samples were prepared in a vacuum system. Liquid 1-ClSiCP was degassed using a freeze-pump-thaw cycle and mixed with host gas (either neon or nitrogen). The matrix mixture was prepared using 0.7 mbar of vapourized 1-ClSiCP and 700 mbar of the matrix gas in the same volume. The mixture was deposited onto a CsI window and kept at the lowest possible temperature of 3 K for the neon matrix and 17 K for the nitrogen matrix in the closed cycle (Janis SHI-4) cryostat. Infrared absorption spectra of the matrix isolated 1-ClSiCP were recorded using a FT-IR spectrometer IFS 120 (Bruker Optik GmbH, Ettlingen, Germany). A KBr beamsplitter, a glowbar source, and a liquid $N_2$ cooled MCT detector were used for spectra acquisition in the 600–4000 $cm^{-1}$ spectral range, with the 1 $cm^{-1}$ spectral resolution, and 256 spectra were averaged for each measurement. The annealing experiments of the sample were performed at 9 K for the neon matrix and 35 K for the nitrogen matrix. After cooling the sample, the spectra were obtained at 3 K (neon) and 17 K (nitrogen). We have chosen the annealing temperatures considering that above a certain point, the diffusion of the title compound is activated, and the matrix isolation effect is lost. At these temperatures, the matrix material can start to evaporate quickly, leading to irreversible changes in the sample.

## RESULTS AND DISCUSSION

### Computational

The type of ring conformation in such ring structures is denoted by a capital letter with the super/subscript numbers, which refer to atoms above/below the ring plane (e.g. $^1E$ is a conformer in the envelope ring conformation with atom number 1 above the ring plane, $^2T_3$ is a conformer in the twisted ring conformation with atom 2 above and atom number 3 below the ring plane) [28]. The axial/equatorial notation describes the position of the substituents with respect to the cycle plane. During the geometry optimisation of 1-ClSiCP, only two stable structures were found, namely $^2T_3$ and $^1E$. The $^2T_3$ conformer was the most stable structure for both calculation methods. The structures are presented in Fig. 1. The vibrational frequency analysis for the $^1E$ conformer revealed the presence of some negative frequency values, which indicates that the calculated structure does not correspond to a local minimum of the potential energy surface but is just a saddle point and such a structure cannot be considered a staggered conformer.

Therefore, the theoretical analysis predicts only one conformer of 1-ClSiCP, having the $^2T_3$ structure. The essential calculated structural parameters of the $^2T_3$ conformer, together with those of the parent compound, 1-chlorosilacyclopentane, are presented in Table 1. Results of the structural calculations are

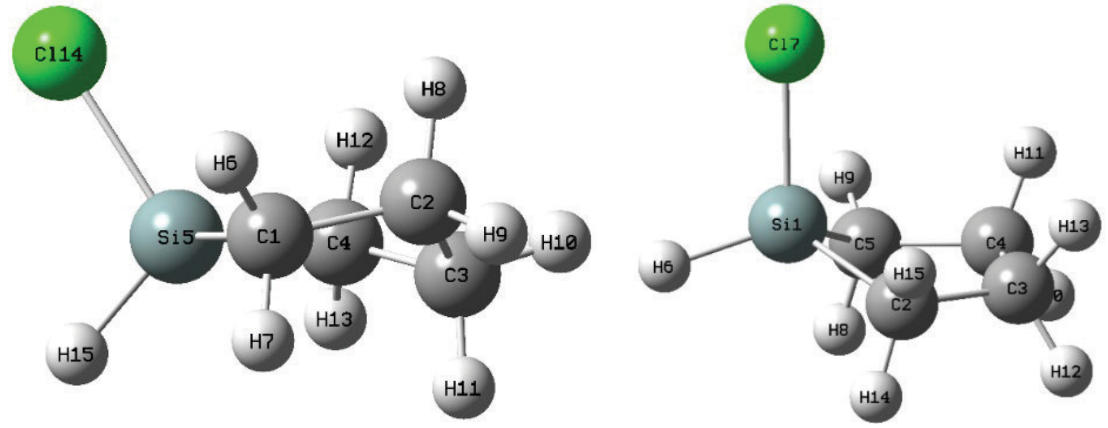

**Fig. 1.** The twisted $^2T_3$ and $^1E$ structure (global energy minimum) and E structure (transition state) of the 1-chlorosilacyclopentane with atom numbering

Table 1. **Comparison of the calculated ring dihedral angles for 1-chlorocyclopentane and 1-chlorosilacyclopentane. The calculations were performed using the B3LYP/aug-cc-pVTZ and MP2/aug-cc-pVTZ methods**

| **1-chlorocyclopentane** | | | | **1-chlorosilacyclopentane** | | | |
|---|---|---|---|---|---|---|---|
| aug-cc-pVTZ | | | | | | | |
| | | B3LYP | MP2 | | | B3LYP | MP2 |
| Dihedral angle value [deg] | $C_1$–$C_2$–$C_3$–$C_4$ | 3 | 0 | Dihedral angle value [deg] | $C_1$–$C_2$–$C_3$–$C_4$ | 49 | 52 |
| | $C_2$–$C_3$–$C_4$–$C_5$ | 20 | 25 | | $C_2$–$C_3$–$C_4$–Si | –35 | –35 |
| | $C_3$–$C_4$–$C_5$–Cl | 82 | 76 | | $C_3$–$C_4$–Si–Cl | 129 | 125 |
| | $C_4$–$C_5$–$C_1$–$C_2$ | –76 | –75 | | $C_4$–Si–$C_1$–$C_2$ | –70 | –69 |
| | $C_5$–$C_1$–$C_2$–$C_3$ | 75 | 77 | | Si–$C_1$–$C_2$–$C_3$ | 53 | 53 |

surprising, since the shapes of the five-membered rings of 1-ClSiCP and 1-chlorocyclopentane are very different. Despite the fact that 1-chlorosilacyclopentane and 1-chlorocyclopentane are closely related compounds differing only in the type of one atom in the ring, this is enough for a large difference in the ring shape (see Table 1) of both compounds: 1-chlorocyclopentane takes an envelope shape, while 1-chlorosilacyclopentane takes a half-chair configuration. Such a difference can be reasoned by the different electronegativities of carbon and silicon atoms present in the rings of these related molecules.

Electronegativity is the tendency for an atom of a given chemical element to attract shared electrons when forming a chemical bond [29]. The different electronegativities of carbon and silicon atoms are caused by their atomic numbers and the distances at which the valence electrons reside from the charged nucleus. The carbon nucleus (atomic number 6) is much smaller than the silicon nucleus (atomic number 14), which makes the electronegativity of carbon higher than that of silicon. The electronegativity values are 2.50 for carbon and 1.8 for silicon [30], and chemical bonds inside the cyclopentane ring should be stronger than those in the silacyclopentane ring, which explains their structural differences. The main difference is that the five-membered ring containing only carbon atoms is flatter than the ring in which a carbon atom is replaced by a silicon atom. For instance, according to B3LYP calculations, the dihedral angle for $C_2$–$C_3$–$C_4$–$C_5$ is equal to 20° while the corresponding angle for $C_2$–$C_3$–$C_4$–Si in 1-chlorosilacyclopentane is equal to 35°. Similar differences in the orientation of the chemical bond connecting the chlorine radical to the rings are also predicted by the calculations.

It is notable that the potential energy minimum for the $^2T_3$ conformer is doubly degenerate, which means that this conformer can be considered as two conformers with the same structure. In this case, transitions between these two structures are possible. Additionally, the vibrational energy levels on both sides of the potential function related to the $C_1$–$C_2$–$C_3$–$C_4$ torsional vibration can interact with each other and cause splitting of energy levels related to such torsional vibration, which can lead to the appearance of additional spectral bands in the vibrational spectra of this compound. This effect depends on the height and width of the potential barriers between these two identical conformers. To investigate this barrier, we performed a Potential Energy Surface Scan for the dihedral angle $C_1$–$C_2$–$C_3$–$C_4$. This scan (see Fig. 2) describes the $^2T_3$ to $^3T_2$ interconversion, with the $^1E$ structure as a transition state. According to the results of the scan, the energy barrier of the $^2T_3/^3T_2$ inversion is equal to 14 kJ/mol and is related to the $^2T_3 \rightarrow {}^1E$ transition. The reverse process, namely $^3T_2 \rightarrow {}^1E$, has the same energy since $^2T_3$ and $^3T_2$ are isoenergetic. The barrier is too high for such a transition to be active at ambient or lower temperatures. Also, splitting of the vibrational spectral bands related to the out-of-plane bending vibration of the $C_1$–$C_2$–$C_3$–$C_4$ group should be extremely small since the vibrational frequency of this vibration is in the range of 67–163 $cm^{-1}$ (see Table 2). This frequency range corresponds to the energy range 0.8–1.95 kJ/mol and is much lower than the 14 kJ/mol barrier. In such conditions, we can neglect the splitting of the energy levels related to the out-of-plane bending vibration of $C_1$–$C_2$–$C_3$–$C_4$ group and exclude the possibility of additional spectral bands in the experimental vibrational spectra of this compound.

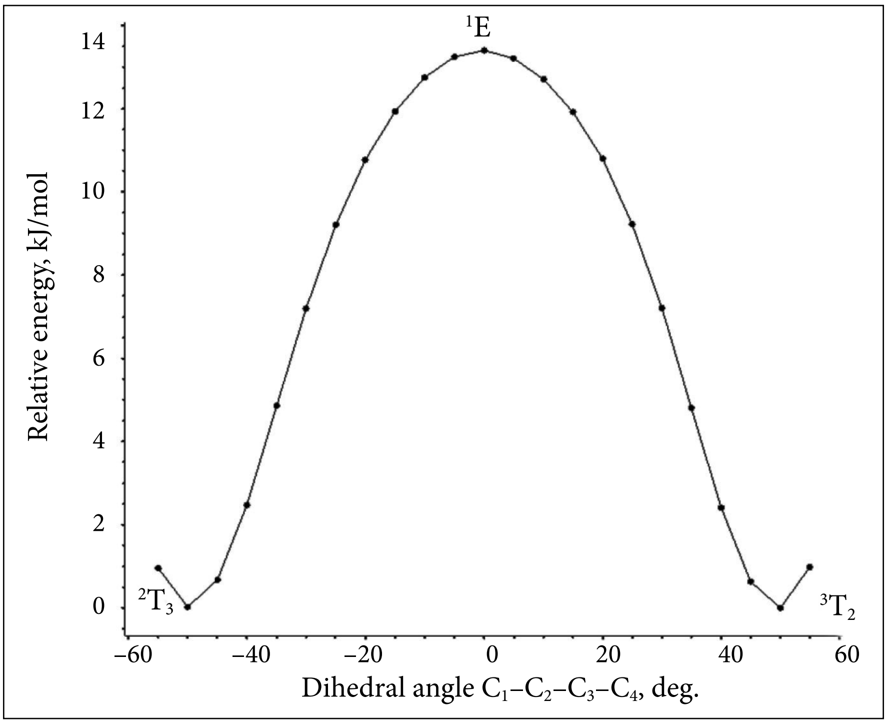

**Fig. 2.** The relaxed potential energy surface scan along the $C_1$–$C_2$–$C_3$–$C_4$ dihedral angle changes obtained from the DFT/B3LYP/aug-cc-pVTZ method. The energy values are presented with respect to the energy value of the lowest conformer for each relaxed surface scan

We have checked theoretical predictions concerning the half-chair configuration of the silacyclopentane ring by comparing the calculated vibrational spectrum of this conformer with the experimental vibrational spectrum of the title compound. The match between the calculated spectrum and the experimental spectrum is very good, what confirms that the structure of the ring of the most stable conformer of 1-chlorosilacyclopentane is in a half-chair form.

## Experimental results

Besides the structural analysis of 1-chlorosilacyclopentane, another task of this work is to make for the first time a complete assignment of the vibrational spectral bands of this compound.

The spectra are presented in Fig. 3. In order to evaluate the stability of the compound over time at ambient conditions, the ATR spectra of a drop of the compound placed on the ATR crystal and naturally exposed to ambient air were recorded

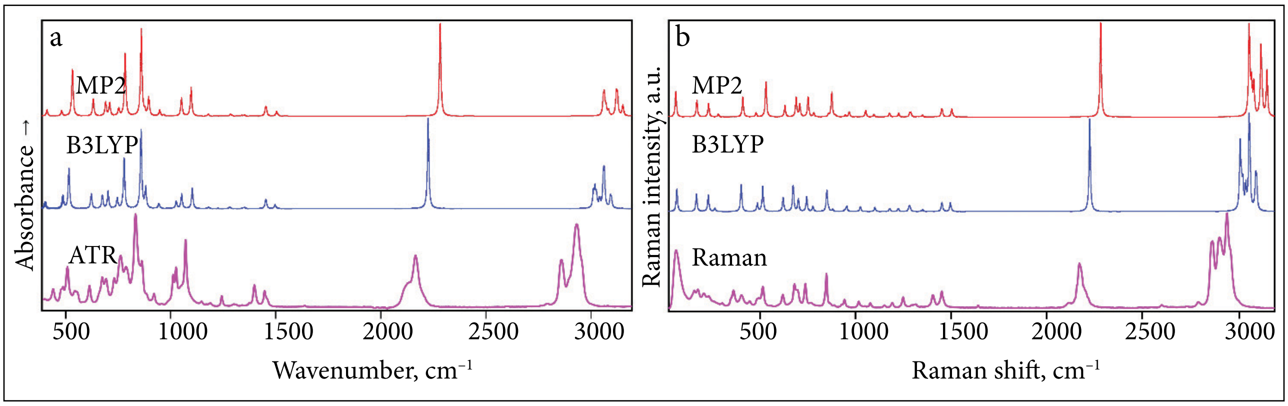

**Fig. 3.** (a) ATR FT-IR absorption spectrum of 1-ClSiCP together with the theoretically DFT/B3LYP/aug-cc-pVTZ and MP2/aug-cc-pVTZ calculated IR absorption spectrum of the $^2T_3$ conformation; (b) Raman spectrum of 1-ClSiCP spectra (pink) together with the theoretically calculated Raman spectra using DFT/B3LYP/aug-cc-pVTZ (blue) and MP2/aug-cc-pVTZ (red) of the $^2T_3$ conformation (DFT/B3LYP/aug-cc-pVTZ)

repeatedly. During 16 min, 16 spectra were captured with a 1 min time interval. Contrary, Raman measurements were recorded in a sealed vial with no contact with air. The ATR IR absorbance and Raman spectra together with the DFT/B3LYP/aug-cc-pVTZ and MP2/aug-cc-pVTZ calculated theoretical spectra are presented in Fig. 3 and the spectral bands are listed in Table 2.

The spectral bands acquired from Raman and ATR experiments exhibit a significant broadening of up to 20 cm$^{-1}$, and in many instances, they overlap, allowing only a tentative assignment. Additionally, the calculations proceeded in the harmonic approximation (see Table 2) do not take into account the anharmonicity of potential functions of the normal vibrations.

Unfortunately, the width of conventional Raman and FT-IR absorption spectra exceeds 20 cm$^{-1}$, which does not allow one to resolve close to each other located spectral bands and to perform the analysis of the normal vibrational modes of the compound or to detect spectral bands belonging to other less abundant conformers of the title compound, if any. The width of the vibrational spectral bands is mainly reasoned by two factors: temperature and intermolecular interactions. Proceeding spectroscopic experiments at ambient temperatures allows for a higher abundance of higher vibrational and rotational energy levels, while in a condensed (liquid or solid) state, intermolecular interactions make such levels broader. In order to reduce the width of the experimental

Table 2. **Experimental ATR IR absorption and Raman spectral bands together with the calculated in harmonic approximation spectral bands of 1-chlorosilacyclopentane. Calculations are performed using the B3LYP/aug-cc-pVTZ and MP2/aug-cc-pVTZ methods**

| Experimental | | | | Calculated | | | | | |
|---|---|---|---|---|---|---|---|---|---|
| | | | | DFT B3LYP/*aug-cc-pVTZ* | | | MP2 *aug-cc-pVTZ* | | |
| Freq [cm$^{-1}$] | IR *I*, a.u. | Freq [cm$^{-1}$] | Raman *I*, a.u. | Freq [cm$^{-1}$] | IR *I*, km/mol | Raman *I*, km/mol | Freq [cm$^{-1}$] | IR *I*, km/mol | Raman *I*, km/mol |
| 2957 | 53 | 2961 | 64 | 3098 | 8 | 30 | 3153 | 6 | 24 |
| | | | | 3093 | 11 | 33 | 3152 | 6 | 35 |
| 2933 | 90 | 2943 | 100 | 3064 | 33 | 25 | 3126 | 19 | 23 |
| | | | | 3059 | 28 | 100 | 3121 | 21 | 79 |
| 2897 | 32 | 2904 | 73 | 3042 | 9 | 26 | 3084 | 5 | 37 |
| 2861 | 53 | 2867 | 68 | 3027 | 13 | 27 | 3072 | 8 | 37 |
| | | | | 3019 | 20 | 24 | 3064 | 20 | 13 |
| | | | | 3012 | 16 | 73 | 3059 | 15 | 100 |
| 2793 | 5 | 2793 | 9 | | | | | | |
| 2602 | 3 | 2602 | 5 | | | | | | |
| 2168 | 58 | 2171 | 46 | 2226 | 100 | 63 | 2283 | 100 | 68 |
| 2130 | 26 | 2114 | 5 | | | | | | |
| 1642 | 3 | 1642 | 5 | | | | | | |
| 1463 | 11 | 1463 | 9 | 1504 | 1 | 0.4 | 1511 | 1 | 0.4 |
| 1451 | 18 | 1452 | 18 | 1497 | 4 | 3 | 1504 | 5 | 3 |
| 1402 | 24 | 1407 | 14 | 1454 | 5 | 2 | 1455 | 6 | 2 |
| 1379 | 5 | 1379 | 4 | 1452 | 6 | 2 | 1451 | 6 | 2 |
| 1315 | 3 | 1315 | 4 | 1352 | 1 | 1 | 1351 | 1 | 1 |
| 1305 | 3 | 1296 | 4 | 1345 | 1 | 0.1 | 1339 | 1 | 0.1 |
| 1270 | 2 | 1269 | 3 | 1286 | 0.3 | 1 | 1290 | 1 | 1 |
| 1249 | 11 | 1250 | 14 | 1281 | 2 | 1 | 1284 | 2 | 1 |
| 1193 | 5 | 1193 | 5 | 1225 | 0.03 | 1 | 1227 | 0.1 | 1 |
| 1151 | 8 | 1151 | 3 | 1180 | 1 | 1 | 1179 | 2 | 1 |

Table 2. **(Continued)**

| **Experimental** | | | | **Calculated** | | | | | |
|---|---|---|---|---|---|---|---|---|---|
| | | | | **DFT B3LYP/*aug-cc-pVTZ*** | | | **MP2 *aug-cc-pVTZ*** | | |
| **Freq [cm$^{-1}$]** | **IR *I*, a.u.** | **Freq [cm$^{-1}$]** | **Raman *I*, a.u.** | **Freq [cm$^{-1}$]** | **IR *I*, km/mol** | **Raman *I*, km/mol** | **Freq [cm$^{-1}$]** | **IR *I*, km/mol** | **Raman *I*, km/mol** |
| 1076 | 74 | 1078 | 5 | 1103 | 22 | 1 | 1097 | 31 | 1 |
| 1031 | 45 | 1033 | 2 | 1052 | 16 | 0.1 | 1054 | 2 | 2 |
| 1017 | 45 | 1017 | 9 | 1026 | 8 | 1 | 1051 | 18 | 0.1 |
| 963 | 5 | 963 | 2 | 955 | 0.2 | 1 | 968 | 1 | 1 |
| 926 | 16 | 943 | 9 | 944 | 6 | 0.3 | 948 | 6 | 0.4 |
| 868 | 50 | 868 | 5 | 881 | 22 | 0.4 | 896 | 20 | 0.3 |
| 839 | 100 | 849 | 32 | 859 | 87 | 0.4 | 877 | 5 | 5 |
| 794 | 45 | | | 851 | 1 | 4 | 860 | 94 | 0.5 |
| 767 | 58 | 767 | 5 | 778 | 56 | 1 | 783 | 67 | 1 |
| 738 | 32 | 738 | 27 | 746 | 11 | 2 | 753 | 8 | 3 |
| 698 | 29 | 698 | 18 | 702 | 19 | 2 | 710 | 14 | 2 |
| 680 | 34 | 683 | 27 | 675 | 14 | 4 | 691 | 15 | 3 |
| 620 | 24 | 620 | 14 | 622 | 16 | 2 | 632 | 18 | 2 |
| 515 | 42 | 515 | 23 | 516 | 44 | 3 | 532 | 50 | 4 |
| 494 | 21 | 494 | 9 | 488 | 14 | 1 | 481 | 6 | 0.4 |
| 485 | 11 | 485 | 9 | | | | | | |
| 447 | 21 | 447 | 9 | 403 | 7 | 2 | 411 | 6 | 2 |
| 233 | 3 | x | x | 266 | 0.3 | 0.2 | 283 | 0.4 | 0.2 |
| 208 | 5 | x | x | 231 | 1 | 1 | 232 | 1 | 1 |
| 178 | 3 | x | x | 169 | 1 | 1 | 171 | 1 | 1 |
| 163 | 8 | x | x | | | | | | |
| 67 | 34 | x | x | 66 | 1 | 0.03 | 61 | 1 | 0.3 |

vibrational spectral bands, the spectroscopic experiments should be performed for the molecules isolated in some inert medium at very low temperatures with suppressed intermolecular interactions.

Usually, the anharmonicity of stretching vibrations is larger than the anharmonicity of bending vibrations, and because of this, the calculated bands are always blue shifted in respect to experimental ones (see Fig. 4). The blue shift can vary from 5 up to 15% and this fact complicates the use of the calculated spectra for the assignment of experimental bands. For a more detailed assignment of the experimental vibrational spectral bands of 1-ClSiCP matrix isolation, FT-IR studies were employed. Two different matrix gases were used – nitrogen and neon. In order to produce homogeneous, non-scattering matrices, rather different deposition temperatures were used: 17 K for nitrogen and 3 K for neon. In conformational analysis, it is common to use matrices that interact with guest molecules. For neon, this interaction is very small while for nitrogen, in the case of polar conformers, it is stronger. It is well known that in the case of a conformational mixture isolated in a nitrogen matrix, polar conformers can be additionally stabilised, and their abundance can be increased. This feature can be used as an additional argument for attributing the spectral bands to various conformers. In order to have a better match between the positions of the experimental spectral bands and the calculated ones, we performed an additional vibrational analysis in the anharmonic approximation utilising DFT/B3LYP/aug-cc-pVTZ. Since every normal vibration consists of a number of internal vibrations,

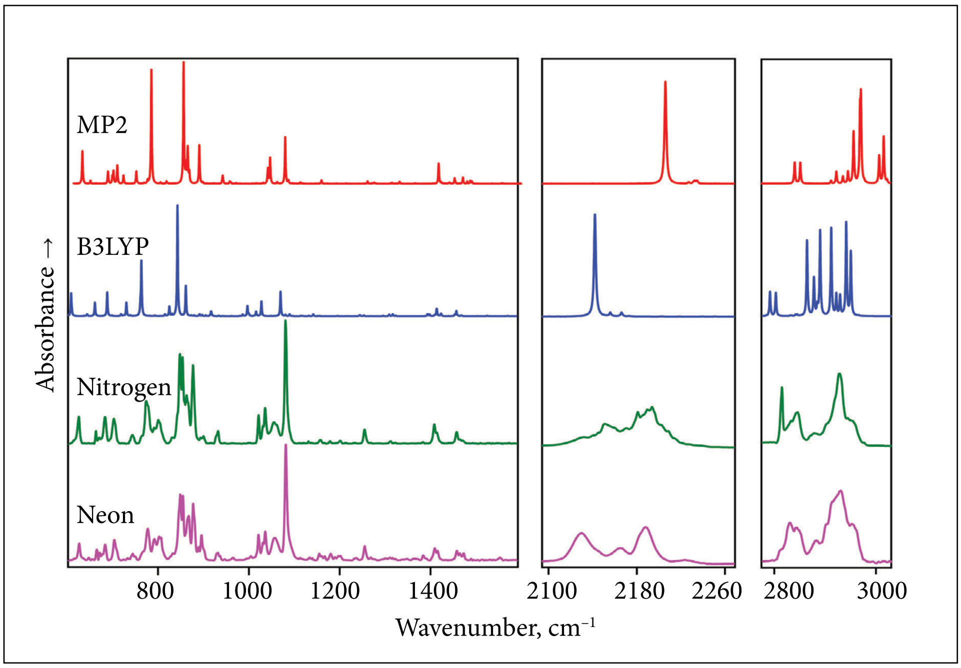

**Fig. 4.** Infrared absorption spectra of 1-ClSiCP isolated in neon at 3 K and nitrogen at 17 K and at the aug-cc-pVTZ theory level in the anharmonic approximation B3LYP and MP2 calculated spectra

the most significant vibrations were determined using the vibrational mode automatic relevance determination (VMARD) program. The nitrogen and neon matrix isolation spectra, together with the anharmonic approximation-calculated IR absorption spectra of 1-ClSiCP, are presented in Fig. 5. Both matrices feature narrow spectral bands, which allow for the separation of closely located spectral bands and make a better assignment. The results of the assignment of matrix spectral bands are presented in Table 4.

The match between the experimental and theoretical spectral bands is good enough, but the presence of some low-energy conformers cannot be

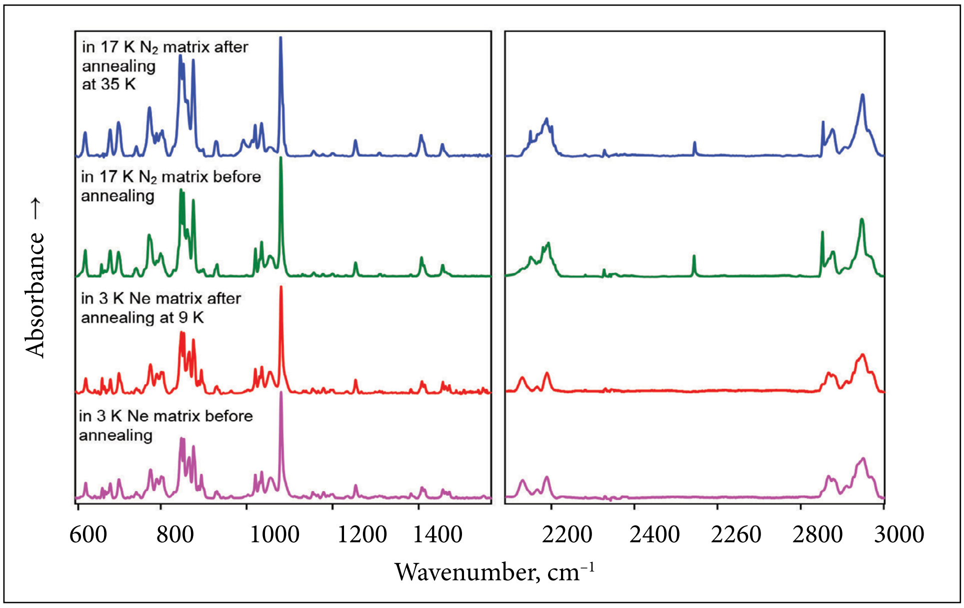

**Fig. 5.** Infrared absorption spectra of 1-ClSiCP isolated in neon at the 3 K (pink) and nitrogen at the 17 K (green) matrix together with the spectra obtained after annealing of the neon matrix at 9 K (red) and after annealing of the nitrogen matrix at 35 K (blue)

Table 3. **Symmetry coordinates used for the description of the normal vibrational modes of 1-ClSiCP**

| | | |
|---|---|---|
| S1 BOND C1 H6 | S31 ANGLE C2 C3 H10 | S61 TORSION C2 C1 Si5 C4 |
| S2 BOND C1 H7 | S32 ANGLE C2 C3 H11 | S62 TORSION C2 C1 Si5 Cl14 |
| S3 BOND C1 C2 | S33 ANGLE C2 C3 C4 | S63 TORSION C2 C1 Si5 H15 |
| S4 BOND C1 Si5 | S34 ANGLE H10 C3 H11 | S64 TORSION C1 C2 C3 H10 |
| S5 BOND C2 H8 | S35 ANGLE H10 C3 C4 | S65 TORSION C1 C2 C3 H11 |
| S6 BOND C2 H9 | S36 ANGLE H11 C3 C4 | S66 TORSION C1 C2 C3 C4 |
| S7 BOND C2 C3 | S37 ANGLE C3 C4 H12 | S67 TORSION C1 Si5 C4 C3 |
| S8 BOND C3 H10 | S38 ANGLE C3 C4 H13 | S68 TORSION C1 Si5 C4 H12 |
| S9 BOND C3 H11 | S39 ANGLE C3 C4 Si5 | S69 TORSION C1 Si5 C4 H13 |
| S10 BOND C3 C4 | S40 ANGLE H12 C4 H13 | S70 TORSION H8 C2 C3 H10 |
| S11 BOND C4 H12 | S41 ANGLE H12 C4 Si5 | S71 TORSION H8 C2 C3 H11 |
| S12 BOND C4 H13 | S42 ANGLE H13 C4 Si5 | S72 TORSION H8 C2 C3 C4 |
| S13 BOND C4 Si5 | S43 ANGLE C4 Si5 Cl14 | S73 TORSION H9 C2 C3 H10 |
| S14 BOND Si5 Cl14 | S44 ANGLE C4 Si5 H15 | S74 TORSION H9 C2 C3 H11 |
| S15 BOND Si5 H15 | S45 ANGLE Cl14 Si5 H15 | S75 TORSION H9 C2 C3 C4 |
| S16 ANGLE H6 C1 H7 | S46 TORSION H6 C1 C2 H8 | S76 TORSION C2 C3 C4 H12 |
| S17 ANGLE H6 C1 C2 | S47 TORSION H6 C1 C2 H9 | S77 TORSION C2 C3 C4 H13 |
| S18 ANGLE H6 C1 Si5 | S48 TORSION H6 C1 C2 C3 | S78 TORSION C2 C3 C4 Si5 |
| S19 ANGLE H7 C1 C2 | S49 TORSION H6 C1 Si5 C4 | S79 TORSION H10 C3 C4 H12 |
| S20 ANGLE H7 C1 Si5 | S50 TORSION H6 C1 Si5 Cl14 | S80 TORSION H10 C3 C4 H13 |
| S21 ANGLE C2 C1 Si5 | S51 TORSION H6 C1 Si5 H15 | S81 TORSION H10 C3 C4 Si5 |
| S22 ANGLE C1 C2 H8 | S52 TORSION H7 C1 C2 H8 | S82 TORSION H11 C3 C4 H12 |
| S23 ANGLE C1 C2 H9 | S53 TORSION H7 C1 C2 H9 | S83 TORSION H11 C3 C4 H13 |
| S24 ANGLE C1 C2 C3 | S54 TORSION H7 C1 C2 C3 | S84 TORSION H11 C3 C4 Si5 |
| S25 ANGLE C1 Si5 C4 | S55 TORSION H7 C1 Si5 C4 | S85 TORSION C3 C4 Si5 Cl14 |
| S26 ANGLE C1 Si5 Cl14 | S56 TORSION H7 C1 Si5 Cl14 | S86 TORSION C3 C4 Si5 H15 |
| S27 ANGLE C1 Si5 H15 | S57 TORSION H7 C1 Si5 H15 | S87 TORSION H12 C4 Si5 Cl14 |
| S28 ANGLE H8 C2 H9 | S58 TORSION Si5 C1 C2 H8 | S88 TORSION H12 C4 Si5 H15 |
| S29 ANGLE H8 C2 C3 | S59 TORSION Si5 C1 C2 H9 | S89 TORSION H13 C4 Si5 Cl14 |
| S30 ANGLE H9 C2 C3 | S60 TORSION Si5 C1 C2 C3 | S90 TORSION H13 C4 Si5 H15 |

neglected. Usually, matrix annealing experiments provide additional arguments about the presence of such conformers. After annealing, the relative intensity of the spectral bands belonging to the most stable conformer should increase, since the conformational thermodynamical equilibrium at 300 K in the freshly deposited matrix is changed to the equilibrium at 17 K (in the case of nitrogen) and 3 K (in the case of neon) after annealing of the matrix. The annealing results are presented in Fig. 5. The spectra of the sample before and after annealing coincides, which allows us to conclude that neither conformational transitions nor the formation of molecular complexes are taking place during the annealing.

The assignment of the experimental spectral bands to the normal vibrations of 1-ClSiCP was performed with the help of vibrational mode automatic relevance determination (VMARD). The calculated vibrational frequencies from the ORCA output were used as input parameters for the vibAnalysis software [31] and VMARD was performed. The symmetry coordinates chosen for the description of the normal vibrations are presented in Table 3.

Since each normal vibration consists of many internal vibrations, only internal vibrations with a significant input into the potential energy are taken into account for the approximate description of the normal vibrational modes.

Table 4. **Assignment of the infrared absorption spectral bands of matrix isolated 1-chlorosilacylcyclopentane using the results of B3LYP/aug-cc-pVTZ and MP2/aug-cc-pVTZ anharmonic calculations for the $^2T_3$ conformer of the title compound**

| Normal vibr. mode | Experimental | | | | Calculated anharmonic | | | | Vibrational mode automatic relevance determination (VMARD) | Approximate description |
|---|---|---|---|---|---|---|---|---|---|---|
| | Ne matrix | | $N_2$ matrix | | B3LYP *aug-cc-pVTZ* | | MP2 *aug-cc-pVTZ* | | | |
| | *ν*, cm$^{-1}$ | *I*, a.u. | *ν*, cm$^{-1}$ | *I*, a.u. | *ν*, cm$^{-1}$ | *I*, km/mol | *ν*, cm$^{-1}$ | *I*, km/mol | | |
| 39 | $2969.1^{sh}$ | 14.8 | $2969.3^{sh}$ | 12.7 | 2966.6 | 21.1 | 3022.3 | 16.9 | 65.6S1 + 18.6S2 + 6.4S5 + 6.1S12 | $\nu_{as}$C(4)H$_2$ |
| 38 | $2951^{br}$ | 51.9 | $2948^{br}$ | 46.0 | 2948.9 | 6.5 | 3014.9 | 9.8 | 51.5S12 + 26.1S11 + 6.9S9 | $\nu_{as}$C(1)H$_2$ |
| 37 | $2936.2^{sh}$ | 29.6 | $2939.5^{sh}$ | 12.7 | 2934.3 | 29.0 | 2984.9 | 21.6 | 31.7S6 + 19.0S5 + 16.7S8 + 12.2S9 + 6.4S12 + 6.0S2 + 5.3S1 | $\nu_{as}$C(2)H$_2$ + $\nu_{as}$C(3)H$_2$ |
| 36 | $2879^{br}$ | 18.5 | $2878^{br}$ | 19.0 | 2916.1 | 28.2 | 2983.4 | 27.1 | 38.3S8 + 23.8S6 + 11.6S11 + 9.7S9 + 8.9S12 + 4.7S2 | $\nu_{as}$C(2)H$_2$ + $\nu_{as}$C(3)H$_2$ + $\nu_s$C(1)H$_2$ |
| 35 | | | | | 2911.4 | 2.8 | 2955.3 | 2.4 | 48.3S11 + 23.8S12 + 16.7S8 + 4.9S9 | $\nu_s$C(4)-H$_2$ |
| 34 | 2865.8 | 22.2 | 2867.9 | 11.1 | 2906.0 | 12.5 | 2944.5 | 4.3 | 36.5S2 + 19.6S5 + 19.0S6 + 12.6S1 + 5.6S8 | $\nu_s$C(4)H$_2$ + $\nu_s$C(3)H$_2$ |
| 33 | | – | 2854.3 | 38.1 | 2843.3 | 7.7 | 2972.8 | 18.5 | 36.2S5 + 26.6S2 + 13.8S6 + 10.3S8 + 7.9S9 + 5.2S1 | $\nu_s$C(3)H$_2$ + $\nu_s$C(2)H$_2$ |
| 32 | | | | | 2833.7 | 8.1 | 2876.0 | 7.6 | 55.2S9 + 18.0S8 + 17.1S5 | $\nu_s$C(2)H$_2$ |
| 31 | 2188.9<br>2164.1<br>2130.4 | 25.9<br>7.4<br>22.2 | 2188.9<br>2158.8<br>2151.2<br>2129.5 | 15.9<br>7.9<br>11.1<br>4.8 | 2142.3 | 100.0 | 2206.3 | 100.0 | 98.4S15 | νSiH |
| 30 | 1472.1<br>1463.8 | 3.7<br>3.7 | – | – | 1466.2 | 0.6 | 1469.3 | 0.5 | 44.4S28 + 23.6S34 + 8.3S40 + 6.5S16 | sc$_s$ CH$_2$ |
| 29 | 1456.8 | 7.4 | 1456.3 | 7.9 | 1455.7 | 3.7 | 1459.8 | 3.6 | 43.6S34 + 25.9S28 | sc$_{as}$ CH$_2$ |
| 28 | 1415.2 | 3.7 | 1413.2 | 6.3 | 1412.6 | 3.4 | 1412.5 | 0.7 | 53.9S40 + 7.7S37 + 6.9S38 + 5.7S28 + 5.6S34 + 4.6S39 | sc C(1)H$_2$ |
| 27 | 1408.4 | 7.4 | 1407.0 | 14.3 | 1411.7 | 0.2 | 1406.4 | 11.4 | 49.8S16 + 7.7S19 + 7.7S17 + 5.9S34 | sc C(4)H$_2$ |
| 26 | – | – | – | – | 1315.7 | 1.5 | 1319.8 | 0.7 | 13.7S29 + 13.4S32 + 12.4S22 + 8.9S36 + 5.5S7 + 4.9S3 + 4.6S17 | *bip*C(2)C(3)H + *bip*C(4)C(1)H |
| 25 | – | – | – | – | 1307.9 | 1.2 | 1303.6 | 0.7 | 11.9S30 + 11.1S31 + 10.9S36 + 8.2S22 + 7.6S32 + 7.5S35 + 7.0S23 + 4.6S29 | $\omega_s$ C(3)H$_2$ + $\omega_s$ C(2)H$_2$ |
| 24 | 1254.1 | 11.1 | 1253.9 | 11.1 | 1252.3 | 0.6 | 1260.1 | 0.3 | 9.8S23 + 7.2S30 + 6.1S20 + 6.0S67 + 6.0S38 + 5.8S22 + 5.0S65 + 5.0S19 + 5.0S37 | tw CH$_2$ |
| 23 | – | – | – | – | 1242.3 | 0.5 | 1249.9 | 1.3 | 12.3S35 + 7.8S24 + 6.9S33 + 5.6S23 + 5.5S37 + 4.8S17 | tw CH$_2$ + $\omega_s$C(4)H$_2$ + $\omega_s$C(1)H$_2$ |
| 22 | 1195.6 | 3.7 | 1199.6 | 1.6 | 1194.6 | 0.2 | 1197.8 | 0.01 | 9.2S19 + 7.4S37 + 5.2S67 + 5.1S32 + 4.8S66 + 4.7S30 + 4.4S38 | ρCH$_2$ + tw CH$_2$ |
| 21 | 1179.1<br>1154.3 | 3.7<br>3.7 | 1177.7<br>1156.5 | 1.6<br>1.6 | 1140.8 | 1.4 | 1148.6 | 1.7 | 8.5S17 + 8.3S38 + 8.0S24 + 7.9S33 + 7.6S42 + 7.2S18 + 6.2S41 + 4.9S20 + 4.6S4 + 4.4S31 + 4.4S13 | $\omega_s$C(1)H$_2$ + $\omega_s$C(4)H$_2$ |
| 20 | 1095.2<br>1080.5 | 3.7<br>100.0 | 1080.0 | 100.0 | 1068.7 | 19.2 | 1068.7 | 26.4 | 9.9S35 + 9.7S17 + 9.6S23 + 8.7S38 + 8.1S18 + 8.1S42 + 6.7S30 + 6.4S31 + 6.1S41 + 6.0S20 | $\omega_s$ C(1)H$_2$ + $\omega_s$ C(4)H$_2$ |
| 19 | 1055.9<br>1035.2<br>$1029.7^{sh}$ | 18.5<br>18.5<br>7.4 | 1052.9<br>1034.9<br>$1029.4^{sh}$ | 14.3<br>25.4<br>6.3 | 1026.7 | 11.7 | 1030.7 | 8.1 | 8.8S38 + 8.0S37 + 5.9S58 + 5.6S41 + 5.3S19 + 4.7S36 + 4.5S22 | tw CH$_2$ |
| 18 | 1020.3 | 18.5 | 1020.4 | 22.2 | 995.9 | 8.0 | 1035.5 | 14.5 | 22.9S7 + 19.7S10 + 18.6S3 + 4.6S73 + 4.5S59 | $\nu_s$ (ring) CC |

Table 4. **(Continued)**

| Normal vibr. mode | Experimental | | | | Calculated anharmonic | | | | Vibrational mode automatic relevance determination (VMARD) | Approximate description |
|---|---|---|---|---|---|---|---|---|---|---|
| | Ne matrix | | $N_2$ matrix | | B3LYP *aug-cc-pVTZ* | | MP2 *aug-cc-pVTZ* | | | |
| | $\nu$, cm$^{-1}$ | $I$, a.u. | $\nu$, cm$^{-1}$ | $I$, a.u. | $\nu$, cm$^{-1}$ | $I$, km/mol | $\nu$, cm$^{-1}$ | $I$, km/mol | | |
| 17 | 928.9 | 3.7 | 930.3 | 9.5 | 932.9 | 0.3 | 949.3 | 0.8 | 13.7S3 + 12.7S10 + 7.9S24 + 6.0S33 + 5.9S17 + 5.5S23 | $\nu_{as}$(ring) CC |
| 16 | 895.1 | 18.5 | 898.8 | 3.2 | 915.9 | 3.4 | 931.0 | 4.4 | 10.5S22 + 6.4S29 + 5.6S20 + 5.4S36 + 5.1S35 + 4.9S16 + 4.8S88 + 4.7S10 + 4.5S42 | tw $CH_2$ |
| 15 | 877.1 | 44.4 | 876.3 | 58.7 | 860.3 | 23.9 | 879.7 | 21.7 | 13.0S3 + 11.5S39 + 11.0S21 + 8.1S31 + 7.6S10 + 7.0S27 + 6.4S35 | $\rho CH_2$ |
| 14 | 865.1<br>854.2<br>847.4 | 33.3<br>40.7<br>51.8 | 862.4<br>853.4<br>847.0 | 31.7<br>47.6<br>63.5 | 841.9 | 87.4 | 857.7 | 6.0 | 7.7S44 + 7.5S24 + 7.1S37 + 6.9S13 + 6.0S32 + 5.3S10 + 5.2S17 + 4.4S45 + 4.4S18 | $\rho CH_2$ |
| 13 | | | | | 830.2 | 1.2 | 845.1 | 68.2 | 18.7S7 + 17.1S10 + 12.9S3 + 6.8S29 | $\nu$ (ring breathing) |
| 12 | 805.9<br>800.0<br>791.1<br>776.3 | 11.1<br>14.8<br>11.1<br>25.9 | 804.1<br>799.2<br>791.0<br>774.9 | 7.9<br>11.1<br>6.3<br>33.3 | 762.5 | 41.2 | 774.2 | 64.5 | 10.6S13 + 10.3S25 + 10.0S27 + 7.0S45 + 5.5S30 + 5.5S23 + 5.3S10 + 4.4S3 | *bip* SiClH |
| 11 | 702.8 | 14.8 | 702.2 | 19.0 | 729.5 | 10.7 | 740.9 | 7.0 | 18.0S4 + 9.2S18 + 8.7S13 + 5.7S45 + 5.7S44 + 5.7S20 + 4.4S21 | *bip* SiClH |
| 10 | 682.7 | 11.1 | 682.2 | 20.6 | 687.3 | 18.8 | 699.2 | 9.8 | 17.6S4 + 6.2S44 + 6.2S41 + 6.0S37 + 5.9S43 + 5.2S39 + 5.0S14 + 4.5S42 + 4.4S33 | *tw* ClSiH |
| 9 | 668.3 | 3.7 | 662.5 | 9.5 | 660.2 | 10.4 | 678.7 | 6.9 | 40.6S13 + 6.8S41 + 6.7S14 + 5.8S10 + 4.7S35 | $\rho CH_2$ |
| 8 | 625.8 | 11.1 | 624.3 | 20.6 | 607.8 | 17.7 | 622.4 | 18.5 | 11.1S4 + 8.9S13 + 8.9S25 + 8.4S3 + 7.1S14 + 5.9S86 + 5.7S66 + 5.2S45 + 4.6S54 + 4.6S85 | $\rho CH_2$ |
| 7 | 485 | * | ** | | 505.7 | 40.9 | 526.3 | 48.8 | 29.4S14 + 9.5S4 + 8.8S24 + 8.0S39 + 5.9S13 | $\rho CH_2$ + *bip* (ring) |
| 6 | 447 | * | ** | | 480.5 | 18.9 | 479.6 | 6.2 | 21.3S14 + 10.3S21 + 8.8S24 + 5.8S4 + 4.9S7 + 4.7S34 | $\rho CH_2$ |
| 5 | 233 | * | ** | | 391.5 | 7.5 | 406.8 | 6.8 | 22.9S25 + 20.7S14 + 8.6S10 + 7.5S3 + 6.7S39 + 5.8S13 + 5.5S26 | $\rho CH_2$ + *bip* (ring) |
| 4 | 208 | * | ** | | 254.2 | 0.4 | 281.2 | 0.3 | 11.7S29 + 8.8S26 + 7.6S22 + 5.9S14 + 4.9S64 + 4.5S46 | $\rho CH_2$ |
| 3 | 178 | * | ** | | 217.5 | 1.0 | 231.7 | 1.0 | 21.3S43 + 18.1S14 + 15.9S26 + 5.7S10 | $\rho CH_2$ + *bop* (ring) |
| 2 | 163 | * | ** | | 155.0 | 1.4 | 172.1 | 1.5 | 15.9S26 + 14.7S43 + 9.6S39 + 7.4S33 + 4.9S62 + 4.5S20 | *bop* (ring) |
| 1 | 67 | * | ** | | 31.0 | 0.5 | 66.6 | 0.6 | 11.6S38 + 10.5S26 + 9.6S43 + 7.6S19 + 7.0S89 + 6.1S42 + 6.1S14 + 5.3S17 + 4.7S50 | *bop* (ring) |

Notes: br, broad; sh, shoulder; ν, stretching; $\nu_s$, symmetric stretching; $\nu_{as}$, asymmetric stretching; *bip*, in-plane bending; *bop*, out-of-plane bending; ρ, rocking; ω, wagging; $\omega_s$, symmetric wagging; $\omega_{as}$, asymmetric wagging; tw, twisting; sc, scissoring; $sc_s$, symmetric scissoring; $sc_{as}$, asymmetric scissoring; a.u., arbitrary units after scaling of the most intense spectral band to 100%. * Intensities of Raman bands are not presented since it is not relevant for the table of IR absorption spectral bands. ** This spectral region is not accessible for the matrix isolation experiments.

According to the theory of normal vibrations of polyatomic molecules, 1-ClSiCP should have 29 normal modes. Since the molecule belongs to the C1 point symmetry group, all normal vibrations should be both – IR absorption and Raman active. Indeed, all the normal modes are visible in the experimental spectrum. The calculations predict the νSiH normal vibration band in the 2130–2189 $cm^{-1}$ spectral range to be the most intense while in the experimental spectrum the most intense band is in the region 1080–1095 $cm^{-1}$. This band corresponds to the $C(1)H_2 + C(4)H_2$ symmetric wagging vibration. Such a discrepancy can be explained by some limitations of the aug-cc-pVTZ basis set used in the calculations. This basis set is known to take into account 4 s orbitals (4 basis functions), 3 sets of p orbitals (3 × 3 = 9 basis functions) and 1 set of d orbitals (5 basis functions) [32, 33] what is not enough for the heavy Si atom and what results in the overestimation of the intensity of νSiH normal vibration spectral band [34]. Deformational vibrations are very sensitive to the orientation of the molecule in the matrix cage and usually they are influenced by the matrix splitting effect. Indeed, the MP2 calculated SiClH bip spectral band at 774 $cm^{-1}$ in the experimental matrix isolation spectra is represented as a set of 4 spectral bands, the calculated $CH_2$ rocking vibration spectral band at 858 $cm^{-1}$ is represented as a set of 3 spectral bands, and the calculated $CH_2$ twisting vibration band at 1030 $cm^{-1}$ is represented as a set of 4 spectral bands. It is notable that in the sets, the bands are separated by 5–15 $cm^{-1}$, which is typical of the matrix splitting effect.

## CONCLUSIONS

For the first time, detailed theoretical calculations of the vibrational spectra of 1-chlorosilacyclopentane were performed using the B3LYP/aug-cc-pVTZ and MP2/aug-cc-pVTZ anharmonic approach. The calculations predict that 1-chlorosilacyclopentane exists only as a single conformer with a twisted ($^2T_3$) ring shape and chlorine in an axial position. This twisted conformer, according to DFT/B3LYP/aug-cc-pVTZ calculations, can be described by two equivalent energy minima, with a potential barrier between them being equal to 14 kJ/mol. The barrier corresponds to the transition state in which 1-chlorosilacylcyclopentane has an $^1E$ structure with all four C atoms of the ring being in one plane. The comparison of ring structures of 1-chlorosilacyclopentane and its parent compound, chlorocyclopentane, reveals that replacing in the five-membered ring one C atom with the Si atom is reasoning change of the shape of the ring from the envelope ($C_s$) to twisted ($C_2$) conformations. This finding can be explained by the different negativity of C and Si atoms constituting the rings.

The perfect match between the calculated IR absorption spectrum and the matrix isolated spectrum of 1-chlorosilacyclopentane confirms the calculation results that in real conditions the substance exists only as a single conformer with a twisted (T) ring shape and chlorine being in an axial position.

## ACKNOWLEDGEMENTS

Authors are thankful for the provided computational time at the High Performance Computing Center (HPCC) of the Lithuanian National Center of Physical and Technology Sciences (NCPTS) at the Physics Faculty of Vilnius University.

Received 13 February 2025
Accepted 5 March 2025

## References

1. S. J. Clarson, J. J. Fitzgerald, M. J. Owen, S. D. Smith, M. E. Van Dyke, *Advances in Silicones and Silicone Modified Materials*, ACS Symposium Series, Vol. 1051, American Chemical Society, WA (2010).
2. J. P. Blitz, C. B. Little, *Fundamental and Applied Aspects of Chemically Modified Surfaces*, The Royal Society of Chemistry (1999).
3. J. El-Maiss, T. Darmanin, E. Taffin de Givenchy, et al., *J. Polym. Sci. Part B Polym. Phys.*, **52**, 782 (2014).
4. A. Rusu, I.-M. Moga, L. Uncu, G. Hancu, *Pharmaceutics*, **15**, 11 (2023).
5. E. Juaristi, *Introduction to Stereochemistry and Conformational Analysis*, John Wiley & Sons, New York (1991).
6. C. Cabre, O. Reiser, *J. Org. Chem.*, **81**, 10109 (2016).
7. J. Jampilek, *Molecules*, **24**, 3839 (2019).
8. H. A. Taha, M. R. Richards, T. L. Lowary, *Chem. Rev.*, **113**, 1851 (2013).
9. K. Nester, K. Gaweda, W. Plazinski, *J. Chem. Theory Comput.*, **15**, 1168 (2019).
10. J. Stocka, R. Platakyte, D. Hickman, et al., *J. Mol. Struct.*, **1272**, 134125 (2023).
11. P. J. M. Swinkels, S. G. Stuij, Z. Gong, et al., *Nat. Commun.*, **12**, 2810 (2021).
12. V. Dragojlovic, *ChemTexts*, **1**, 14 (2015).

13. I. O. C. Ekejiuba, H. E. Hallam, *Spectrochim. Acta Part Mol. Spectrosc.*, **26**, 59 (1970).
14. I. O. C. Ekejiuba, H. E. Hallam, *Spectrochim. Acta Part Mol. Spectrosc.*, **26**, 67 (1970).
15. J. R. Durig, A. M. E. Defrawy, A. Ganguly, T. K. Gounev, G. A. Guirgis, *J. Phys. Chem. A*, **113**, 9675 (2009).
16. J. R. Durig, S. S. Panikar, K. A. Glenn, Y. Y. Zheng, G. A. Guirgis, *Vib. Spectrosc.*, **55**, 250 (2011).
17. G. A. Guirgis, S. S. Panikar, J. J. Klaassen, S. S. Purohit, M. D. Johnston, J. R. Durig, *Spectrochim. Acta A Mol. Biomol. Spectrosc.*, **79**, 858 (2011).
18. C. A. Stortz, A. M. Sarotti, *RSC Adv.*, **9**, 24134 (2019).
19. S. Bell, H. D. Stidham, A. J. LaPlante, Y. Y. Zheng, G. A. Guirgis, *J. Mol. Struct.*, **992**, 1 (2011).
20. J. Stocka, R. Platakyte, T. M. C. McFadden, et al., *J. Mol. Struct.*, **1249**, 131644 (2022).
21. T. M. C. McFadden, R. Platakyte, J. Stocka, et al., *J. Mol. Struct.*, **1221**, 128786 (2020).
22. J. Stocka, J. Čeponkus, V. Šablinskas, P. Rodziewicz, *Spectrochim. Acta A Mol. Biomol. Spectrosc.*, **238**, 118425 (2020).
23. F. Neese, *Wiley Interdiscip. Rev. Comput. Mol. Sci.*, **8**, e1327 (2017).
24. A. D. Becke, *J. Chem. Phys.*, **98**, 5648 (1993).
25. T. H. Dunning Jr., *J. Chem. Phys.*, **90**, 1007 (1989).
26. M. J. Frisch, G. W. Trucks, H. B. Schlegel, et al., *Gaussian 16, Revision C.01*, Gaussian, Inc., Wallingford, CT (2019).
27. S. Bell, H. D. Stidham, A. J. LaPlante, Y. Y. Zheng, G. A. Guirgis, *J. Mol. Struct.*, **992**, 1 (2011).
28. J. C. P. Schwarz, *J. Chem. Soc. Chem. Commun.*, **14**, 505 (1973).
29. P. F. Lang, *J. Chem. Educ.*(2024).
30. J. J. Petkowski, W. Bains, S. Seager, *Life*, **10**, 84 (2020).
31. F. Teixeira, M. N. D. S. Cordeiro, *J. Chem. Theory Comput.*, **15**, 456 (2019).
32. N. Sylvetsky, M. K. Kesharwani, J. M. L. Martin, *J. Chem. Phys.*, **147**, 134106 (2017).
33. H. Åström, S. Lehtola, *J. Phys. Chem. A*, **127**, 10872 (2023).
34. W. Beyer, M. S. Abo Ghazala, *MRS Online Proc. Libr.*, **507**, 601 (1998).

**J. Mačytė, J. Lach, R. Platakytė, J. Čeponkus, V. Aleksa, M. Ali, V. Šablinskas, P. Rodziewicz, G. A. Guirgis**

## 1-CHLORSILACIKLOPENTANO STRUKTŪRINĖ ANALIZĖ NAUDOJANT VIRPESINĘ SPEKTROSKOPIJĄ

*Santrauka*

Naujai susintetinto junginio, 1-chlorsilaciklopentano (1-ClSiCP), struktūra buvo tiriama taikant virpesinę spektroskopiją ir teorinius skaičiavimus. Skystos agregatinės būsenos mėginys buvo analizuojamas ATR FT-IR ir Ramano sklaidos spektroskopija. 1-ClSiCP buvo tiriama žemos temperatūros matricinės izoliacijos infraraudonosios sugerties spektriniu metodu. Spektrinių duomenų analizė buvo atlikta taikant du teorinius metodus – tankio funkcionalo teoriją (DFT) ir *ab initio* skaičiavimus. 1-ClSiCP izoliuoto Ne ir $N_2$ matricose FT-IR spektrai buvo registruoti prieš ir po matricos atkaitinimo. Atliekant teorinę struktūrinę analizę buvo tiriamos tik dvi konformacijos, kurioms būdinga Cl radikalo *axial* ir *equatorial* orientacijos bei penkianario žiedo *envelope* ir *twist* konformacijos. Skaičiavimai buvo atlikti naudojant MP2 ir DFT teorinius metodus su aug-cc-pVTZ elektronų Gauso funkcijų baze. Potencinį konformacinio virsmo barjerą atitinkanti molekulės struktūra yra *envelope* tipo ir ji buvo nustatyta atliekant potencinės energijos paviršiaus skenavimą. Eksperimentiniai spektriniai rezultatai patvirtino, kad šiai molekulei egzistuoja tik viena stabili konformacija (*twist*). Gretinant su teoriniais eksperimentinius matricinės izoliacijos IR spektrinius rezultatus, gautus naudojant anharmoninį artinį, nustatyta, kad spektrų sutapimas yra geras ir poslinkiai tarp teorinių ir eksperimentinių spektrinių juostų padėčių neviršija 2 %.